Christoph Kern
Andreas Jess*

Pore Diffusion in the Fischer–Tropsch Synthesis: Limitation or Advantage in Multi-Tubular Reactors?

The Fischer–Tropsch synthesis (FTS) is a highly exothermic reaction often conducted in multi-tubular fixed-bed reactors. Pore diffusion limitations within the catalyst particles are typically viewed as detrimental due to reduced reaction rates. However, this study demonstrates that these limitations can provide significant benefits in terms of reactor stability and performance. Using a 2D numerical reactor model, we explore the influence of pore diffusion on temperature profiles, conversion, and thermal runaway behavior under realistic operating conditions. Results reveal that pore diffusion reduces the apparent activation energy, effectively mitigating thermal sensitivity and increasing the allowable level of reaction temperature. Consequently, higher CO conversions can be achieved safely compared to an idealized scenario without pore diffusion limitations. Hence, pore diffusion limitations, rather than being a disadvantage, act as a stabilizing factor in FTS reactors.

Supporting Information available online

Keywords: Fischer–Tropsch synthesis, Multi-tubular reactor, Pore diffusion limitations

Received: February 04, 2025; *revised:* May 14, 2025; *accepted:* May 20, 2025

DOI: 10.1002/ceat.70049

1 Introduction

For Fischer–Tropsch synthesis (FTS), multi-tubular reactors are commonly used to regulate reaction temperatures and ensure safe operation, minimizing the risk of thermal runaway. These reactors cool up to 10 000 tubes, each typically measuring 2–5 cm in diameter, by circulating boiling water around them.

The risk of thermal runaway necessitates the analysis of reactor behavior using computer simulations based on reliable mathematical models. These models should accurately predict temperature and concentration profiles across various design and operational parameters, such as tube diameter and cooling temperature. 2D models are commonly utilized to address axial and radial temperature gradients within the fixed-bed. This 2D approach is recommended for accurately predicting runaway, as opposed to 1D model, where heat transport resistances are simplified and lumped at the tube wall [1–5].

In a multi-tubular FTS reactor and other fixed-bed reactors, catalyst particles typically have diameters in the millimeter range to avoid excessive pressure drop. However, this design often results in pore diffusion limitations, which significantly reduce the effective reaction rate compared to the intrinsic rate. In FTS, this occurs because the catalyst pores are filled with liquid hydrocarbons (HCs), and the diffusion coefficients for CO and H_2 in liquid HCs are relatively low ($D_{liq} \approx 0.01\, D_{gas}$) [5–11].

Although pore diffusion limitations are often considered an unavoidable drawback—as they lower the effective reaction rate compared to the intrinsic rate—they also provide certain advantages:

1. The apparent activation energy is approximately halved (at least for $\eta_{pore} < 0.5$), which reduces the thermal sensitivity of the reactor.
2. The permissible temperature difference between the maximum tube center temperature and the cooling temperature can increase by a factor of two to three, enhancing reactor stability.
3. The cooling temperature required to avoid runaway is generally higher with pore diffusion limitations, enabling operation at higher temperatures, at least, as discussed below for FTS, if the maximum temperature is not limited by other constraints such as selectivity, catalyst stability, etc.

In previous studies, we introduced a detailed 2D model for a cooled FTS fixed-bed reactor using a cobalt catalyst [6–10]. This model is now applied to investigate the specific impact of pore diffusion limitations on reactor behavior, particularly in terms of achievable syngas conversion and safety margins against thermal runaway.

This study aims to address the following questions:

1. What is the impact of pore diffusion limitations on the sensitivity and runaway behavior of a cooled fixed-bed FTS reactor?

Christoph Kern, Andreas Jess (jess@uni-bayreuth.de)
Chair of Chemical Engineering, Center of Energy Technology, University of Bayreuth, Universitätsstraße 30, 95440 Bayreuth, Germany.

2. Are pore diffusion limitations generally a disadvantage, or could they be advantageous for syngas conversion and HC production in multi-tubular FTS reactors?
3. What roles do tube diameter, intrinsic activity, and cobalt content play under these conditions?

Although this work focuses on FTS, the conclusions are broadly applicable to other heterogeneously catalyzed, exothermic reactions that are diffusion limited and conducted in cooled fixed-bed reactors.

This study only very briefly discusses the general aspects of FTS, intrinsic and effective kinetics on cobalt catalysts, and the characteristics of the 2D model used in this study. Detailed information, including rate equations and mass/heat transfer correlations, is available in previous works [6–10].

2 Methodology: Kinetics of FTS and Multi-Tubular FTS Reactor Model

2.1 Intrinsic and Effective Reaction Kinetics of FTS

The primary reaction of FTS, leading predominantly to paraffinic C_{2+}-HCs, is as follows:

$$CO + 2H_2 \rightarrow (-CH_2-) + H_2O \quad \Delta_R H_{CH_2}{}^0{}_{298} = -152\,\mathrm{kJ\,mol^{-1}} \tag{1}$$

For a reliable kinetic description of FTS, methane formation should be treated separately:

$$CO + 3H_2 \rightarrow CH_4 + H_2O \quad \Delta_R H_{CH_4}{}^0{}_{298} = -206\,\mathrm{kJ\,mol^{-1}} \tag{2}$$

The intrinsic rates for methane ($r_{m,CO,CH4}$) and C_{2+}-HCs ($r_{m,CO,C2+}$), along with internal diffusion limitations, have been experimentally determined in prior studies for Pt promoted (0.03 wt% Pt for Co reduction) Co/γ-Al_2O_3 catalysts with a Co content of 10 wt% [12–16]. Both rates adhere to Langmuir–Hinshelwood kinetics, accounting for the influences of CO and H_2 concentrations. Details on the kinetics both on cobalt and iron catalyst can be found in a recent review [17].

The total intrinsic rate combines these rates, as CO_2 formation by water–gas shift is minimal for Co catalysts:

$$r_{m,\,CO} = -\frac{d\dot{n}_{CO}}{dm_{cat}} = C_A\left(r_{m,\,CO,\,CH_4} + r_{m,\,CO,\,C_{2+}}\right) \tag{3}$$

In Eq. (3), the activity coefficient C_A reflects the CO content and intrinsic activity, with the baseline of one for 10 % CO. Increasing the CO content enhances C_A. FTS catalysts typically contain up to 30 wt% CO ($C_a \approx 3$), and this limiting value is assumed in this study, varying C_A in a range of 0.5–3.

A steam inhibition is also considered, and our experiments indicate [8]:

$$r_{m,\,CO,\,H_2O} = r_{m,\,CO}\left(1 - \frac{c_{H_2O}}{472\,\mathrm{mol\,m^{-3}}}\right) \tag{4}$$

A value of c_{H_2O} of 120 mol m^{-3}, corresponding to a CO conversion of 40 % and a partial pressure of steam of about 5 bar (30 bar, syngas with 31 % CO and 69 % H_2), reduces the reaction rate by 25 %.

Eqs. (3) and (4) reflect only the intrinsic rate. However, pore diffusion limitations lead to a reduced effective rate for millimeter-sized particles to mitigate excessive pressure drop. The effective rate, incorporating the pore effectiveness factor η_{pore} (details to calculate η_{pore} in [6–9]), is given by:

$$r_{m,\,CO,\,eff} = \eta_{pore}\, r_{m,\,CO,\,H_2O} \tag{5}$$

As outlined in [6, 7], the effectiveness factor η_{pore} and the related Thiele modulus ϕ are:

$$\eta_{pore} = \frac{r_{m,\,CO,\,eff}}{r_{m,\,CO}} = \frac{\tanh\phi}{\phi} \approx \frac{1}{\phi} \text{ for } \phi > 2 \tag{6}$$

$$\phi = \left\{\frac{d_p}{6}\sqrt{\frac{\rho_{cat}}{D_{eff,CO,liq}\frac{R\,T}{H_{CO}}}}\right\}\sqrt{\frac{r_{m,CO,H_2O}}{c_{CO}}} = C_\phi\sqrt{\frac{r_{m,CO,H_2O}}{c_{CO}}} \tag{7}$$

The value of the almost constant factor C_ϕ for a particle diameter of 3 mm is 300 $kg^{0.5}\,s^{0.5}\,m^{-1.5}$.

η_{pore} is significantly affected by temperature. For the particle diameter d_p of 3 mm assumed here, η_{pore} is below one above 180 °C, dropping to 0.2 for 240 °C and $C_a = 3$ [9, 10]. This leads to a higher molar H_2-to-CO ratio in the particles relative to the bulk phase, typically two, enhancing undesired CH_4 formation over C_{2+}-HCs as the diffusion coefficient of H_2 in liquid HCs is double that of CO. This effect intensifies above 240 °C, with CH_4 selectivity surpassing 20 % versus 10 % in absence of diffusion limitations. Hence, in this work the maximum temperature was limited to 240 °C [5–16].

These (negative) effects on product selectivity observed at Thiele modulus values above about one ($\eta_{pore} < 0.75$) are also reported by Bukur et al. [18] and Iglesia et al. [19] for cobalt as catalyst. It is beyond the focus of our study to consider this negative selectivity effect of internal diffusion limitations. Instead, we focus only on the impact of internal diffusion limitations on the effective reaction rate, activation energy, and above all on reactor sensitivity regarding thermal runaway, as discussed below. These three parameters are practically not affected by selectivity issues. Hence, we have here simplifying assumed a constant methane selectivity of 20 %, although without pore diffusion limitations, this value may be lower (e.g., 10 %).

2.2 2D Model of Cooled Multi-Tubular Fixed-Bed FTS Reactor

In addition to intrinsic and effective kinetics, the 2D-reactor model used in this study incorporates the following key aspects:

1. The heat released during FTS radially dissipates in the pseudo-homogeneous phase, comprising both catalyst and gas within the reactor bed, to the tube wall. This process is governed by the radial thermal conductivity (λ_{rad}).
2. Near the inner tube wall, the heat transfer coefficient ($\alpha_{w,int}$) accounts for thermal resistance caused by the high porosity of the bed near the wall. This results is in a temperature discontinuity or "jump" at the wall.
3. Heat is transferred through the tube wall by conduction, which contributes minimally to the overall thermal resistance and subsequently to the cooling fluid (boiling water), as determined by the external heat transfer coefficient ($\alpha_{w,ex}$).

Table 1. Main results of reactor modeling for $d_{t,int} = 3$ cm, $T_{cool} = 211$ °C, and $C_a = 2$.

Final conversion of CO X_{CO} at $z = 12$ m (=X_{H2})	47.5 %
Maximum axial temperature T_{max} (at $r = 0$) reached at $z = 2.3$ m	235.7 °C
Conversion of CO reached at $z = 2.1$ m $X_{CO,\,2.1\,m}$ (=$X_{H2,\,2.1\,m}$)	10.2 %
Ignition temperature (runaway) $T_{cool,\,crit}$	216 °C
Pore effectiveness factor η_{pore} (at T_{max}, $z = 2.3$ m, $r = 0$)	0.32
Radial dispersion parameter/coefficient $\varepsilon_{bed}\,D_{rad}$	1.5×10^{-4} m^2 s^{-1} [20–29]
Effective radial thermal conductivity λ_{rad} (at T_{max}, $z = 2.3$ m)	4.2 W m^{-1} K^{-1} [30, 31]
Internal heat transfer coefficient (bed to internal tube wall) $\alpha_{w,int}$ ($z = 2.3$ m)	999 W m^{-2} K^{-1} [32, 33]
External heat transfer coefficient (external wall to boiling water) $\alpha_{w,ex}$ ($z = 2.3$ m)	1508 W m^{-2} K^{-1} [33–36]
Radial heat flux (wall to boiling water) $\dot{q}$ (at T_{max}, $z = 2.3$ m)	5564 W m^{-2} [33–36]
Pressure drop Δp_{bed}	1.16 bar [37]

4. The adiabatic temperature increase due to the FTS reaction can reach up to 2000 K for complete CO conversion with pure CO and H_2 as syngas. However, the permissible increase to avoid thermal runaway is typically limited to below 30 K, necessitating effective cooling. This study employs tubes with diameters of 1.5 and 3 cm. Although a 1.5 cm diameter is not practical for industrial reactors (due to the very high number of required tubes, $\sim 1/d_t^2$), it is included here to investigate a border scenario with a rather high cooling intensity.
5. Changes in the molar flow rate and pressure drop are included in the model, as they influence gas velocity and residence time.
6. Radial dispersion of mass is considered, although its impact on reactor performance is minimal [10]. Axial dispersion of mass and heat is neglected, as it predominantly affects systems with steeper axial gradients over very short distances [9].
7. This study does not account for syngas recycling in order to concentrate only on the influence of pore diffusion limitations. The syngas consists only of H_2 and CO, with a fixed H_2-to-CO ratio of 2.2. This setup ensures identical H_2 and CO conversions and corresponds to a methane selectivity of 20 %.
8. The differential equations (DEs) for mass and heat balances are solved using the Presto Kinetics software, a reliable solver for DEs (CiT GmbH, Rastede, Germany).

Results from reactor modeling, including the effects of pore diffusion under typical conditions ($d_{t,int} = 3$ cm, $T_{cool} = 211$ °C, $C_a = 2$), are presented in Tab. 1. Operational conditions and details of the chemical media are provided in Supporting Information Tab. S1.

3 Simulation of FTS Reactor with and without Considering Pore Diffusion Limitations

Fig. 1 illustrates the significant impact of reaction temperature and activity coefficient (C_a) on the pore effectiveness factor (η_{pore}) for temperatures ranging from 220 to 250 °C and values of C_a between 0.5 and 3 (corresponding to 5–30 wt% CO). The Thiele modulus increases substantially with temperature due to the almost exponential rise in CO conversion rate and is proportional to $C_a^{0,5}$ (see Eqs. (3) and (7)). For realistic values of C_a greater than one (CO content = 10 wt%), and at temperatures above 230 °C, the intrinsic reaction rate exceeds the effective rate by a factor of two ($\eta_{pore} = 0.5$) to five ($\eta_{pore} = 0.2$).

Figs. 2 and 3 illustrate axial temperature profiles and the corresponding CO conversion for different cooling temperatures, considering tube diameters of 3 and 1.5 cm, while accounting for realistic pore diffusion limitations ($\eta_{pore} < 1$) to emphasize the influence of pore diffusion.

For a tube diameter of 3 cm, the allowable cooling temperature is limited to 205 °C to prevent thermal runaway, maintaining a safety margin of 5 K below the ignition temperature, as depicted in the lower part of Fig. 2. The maximum axial temperature at this cooling temperature reaches 230 °C at a tube length of approximately 3 m. This is still 10 K below the critical maximum of 240 °C, necessary to avoid excessive methane formation.

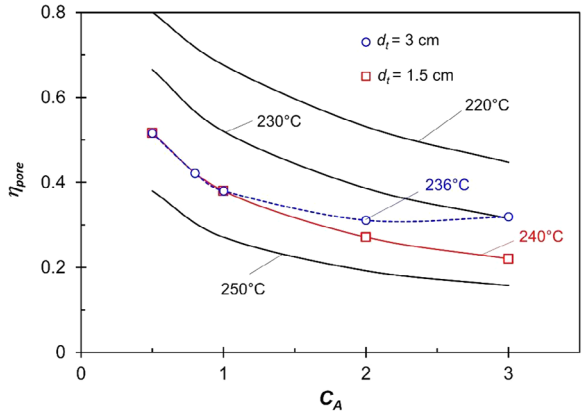

Figure 1. Influence of temperature and activity coefficient C_a on the pore effectiveness factor η_{pore} in a temperature range of 220–250 °C (conditions as listed in Tab. 1 and Supporting Information Tab. S1). The values indicated in red and blue are the respective maximum allowable temperatures, as explained below in further detail.

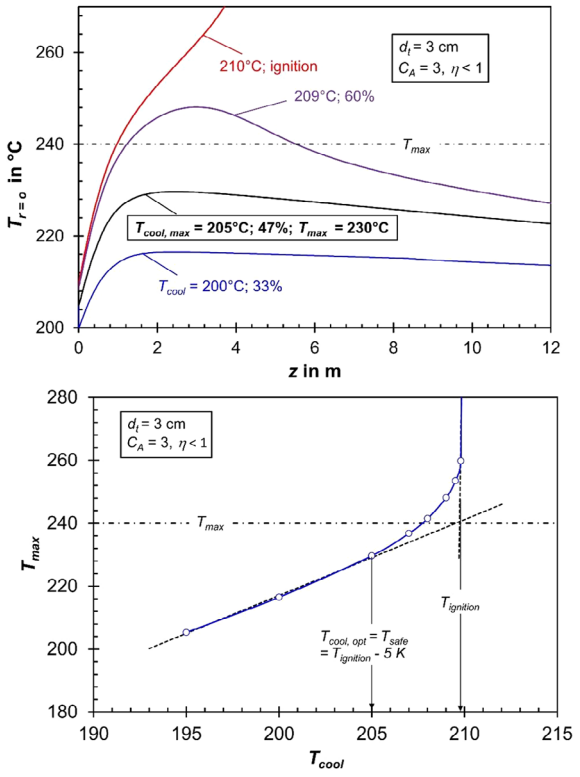

Figure 2. Top: Axial temperature profiles for an internal tube diameter of 3 cm, a high activity coefficient C_A of 3 (30 wt% CO), and "realistically" considering pore diffusion limitations. Bottom: Influence of T_{cool} on maximum axial temperature reached in tube center at $r = 0$ (reactor conditions as listed in Tab. 1 and Supporting Information Tab. S1). The corresponding diagram $T_{max} = f(T_{cool})$ for a low C_A of 1 and a low tube diameter of 1.5 cm is shown in Supporting Information Fig. S1.

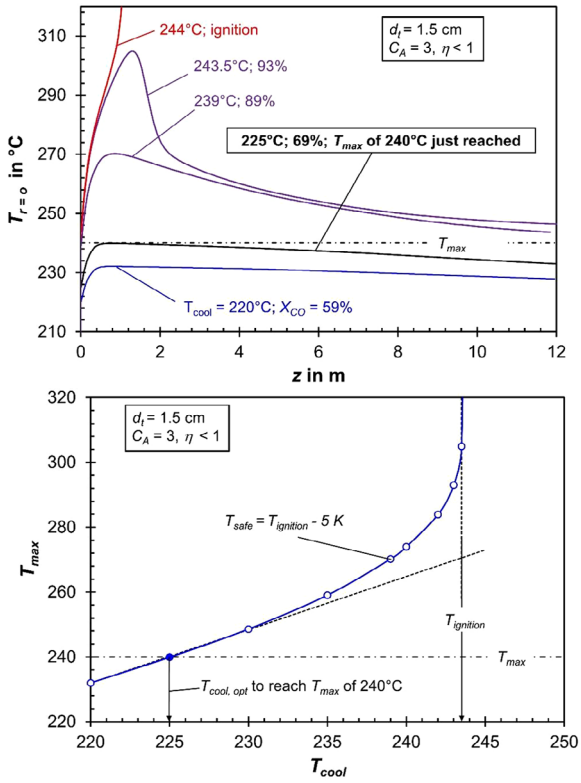

Figure 3. Top: Axial temperature profiles for an internal tube diameter of 1.5 cm and a high activity coefficient C_A of 3 (30 wt% CO), and "realistically" considering pore diffusion limitations. Bottom: Influence of cooling temperature on maximum axial temperature reached in the center of the tube at $r = 0$ (other reaction/reactor conditions as listed in Tabs. 1 and 2). The respective diagram "T_{max} versus T_{cool}" for the case of $C_A = 1$ is shown in Supporting Information Fig. S1; ignition then occurs not before versus $T_{cool} = 263$ °C.

For the smaller tube diameter of 1.5 cm (Fig. 3), and thus a higher cooling intensity enabled by the increased tube area-to-volume ratio, ignition "delays" until the cooling temperature reaches 244 °C. Under these conditions, the allowable cooling temperature increases to 239 °C, corresponding to a maximum reaction temperature of 270 °C and a CO conversion approaching 90% (Fig. 3, bottom). However, to ensure that the reaction temperature remains within the permissible limit of 240 °C (to avoid a too high methane selectivity), the cooling temperature must be reduced to 225 °C. This adjustment limits the reaction temperature to exactly 240 °C in the front section of the tubes but lowers the CO conversion from about 90 % to 69 % (Fig. 3).

If we consider the hypothetical scenario where pore diffusion limitations are completely absent ($\eta_{pore} = 1$), for instance, if the pores were not be filled with liquid HCs, the situation changes significantly (Fig. 4). For a tube diameter (d_t) of 3 cm and a high activity coefficient ($C_A = 3$), ignition already occurs at a low cooling temperature of approximately 193 °C. Even for smaller tubes ($d_t = 1.5$ cm) and a relatively low intrinsic activity ($C_A = 1$), the maximum allowable cooling temperature ($T_{cool, max}$) reaches 221 °C. The corresponding axial temperature profiles and CO conversion rates for various cooling temperatures are provided in Supporting Information Figs. S2 and S3.

For the first and highly critical case ($C_A = 3$, $d_t = 3$ cm), the cooling temperature is limited to 188 °C (5 K below ignition) to prevent thermal runaway (Fig. 4, top). Under these conditions, the maximum axial temperature is just 195 °C, and the CO conversion remains very low at 14 % (Supporting Information Fig. S3). In contrast, for the realistic case where pore diffusion limitations are present ($T_{cool} = 205$ °C, $T_{max} = 230$ °C), the CO conversion increases significantly to 47 % (Fig. 2). Thus, the unavoidable limitation due to pore diffusion proves to be a clear advantage in this scenario.

For the less critical case of a low activity combined with a low tube diameter ($C_A = 1$, $d_t = 1.5$ cm), the absence of pore diffusion limitations limits T_{cool} to 217 °C (Fig. 4, bottom). Even then, the maximum axial temperature is 226 °C, well below the permissible limit of 240 °C. The CO conversion under these conditions reaches 44 % (Supporting Information Fig. S2). However, this is still lower compared to the realistic scenario with pore diffusion limitations ($T_{cool} = 230$ °C, $T_{max} = 240$ °C, $X_{CO} = 49$ %, see Supporting Information Fig. S1).

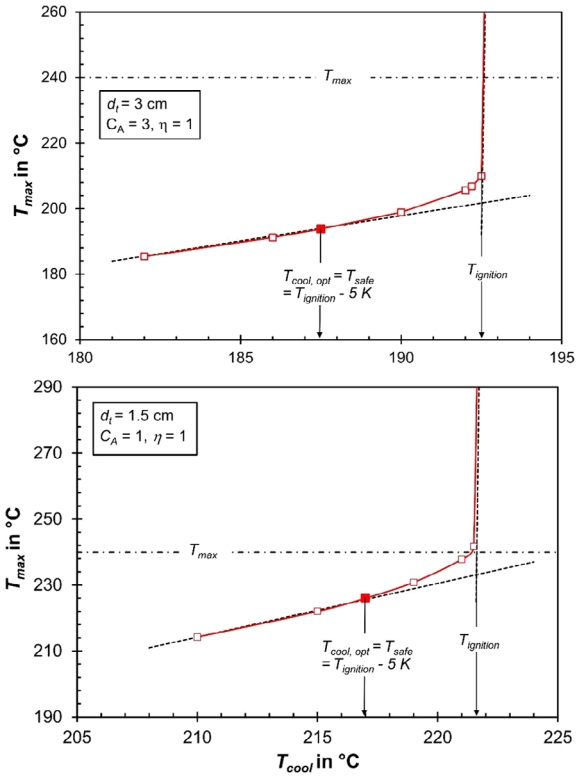

Figure 4. Influence of cooling temperature on maximum axial temperature reached in the center of the tube at $r = 0$ in the hypothetical case without pore diffusion limitations, i.e., $\eta_{pore} = 1$. Top: Internal tube diameter of 3 cm and rather high activity coefficient C_A of 3 (30 wt% CO). Bottom: Small diameter of 1.5 cm and low C_A of 1. The corresponding axial temperature profiles and degrees of CO conversion are shown in Supporting Information Figs. S2 and S3.

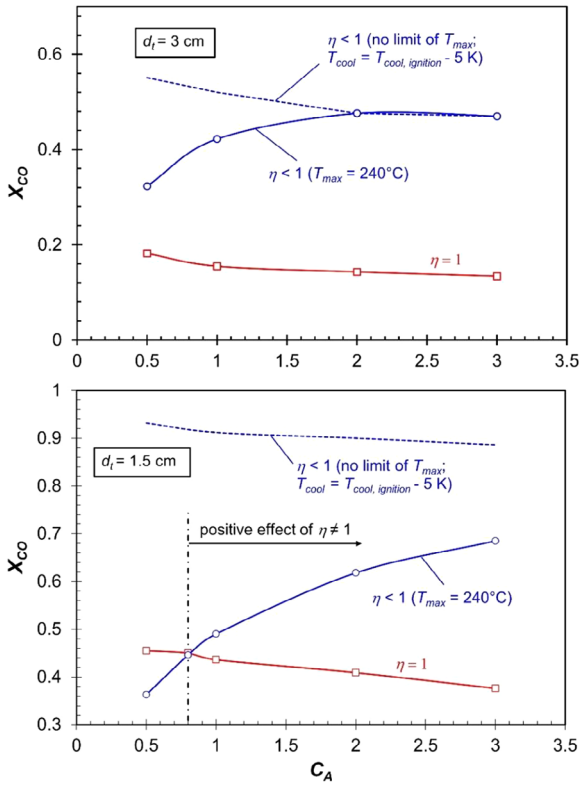

Figure 5. Influence of activity coefficient C_A on achievable conversion of CO (and H_2), if the maximum cooling temperature is set to be 5 K lower than the ignition temperature for a tube diameter of 3 cm (top) and 1.5 cm (bottom). Blue: Realistic consideration of influence of pore diffusion on effective reaction rate; red: hypothetical case without pore diffusion limitations. This is also illustrated in Supporting Information Fig. S5 by the respective values of the intrinsic reaction rate and the effective rate, respectively, reached at the axial position of the temperature maximum (center of tube at $r = 0$). The corresponding cooling temperatures and maximum axial temperatures are shown in Fig. 6. Blue dashed lines: CO conversion in case of pore diffusion limitations, if the limit of the maximum temperature is not set to 240 °C to avoid a high methane selectivity.

Fig. 5 demonstrates that, in most cases, pore diffusion limitations are (on first sight unexpectingly) advantageous and can be even considered a fortunate circumstance regarding the achievable CO conversion. This holds here for FTS true across a wide range of catalytic activities and tube diameters. Only in cases with a small tube diameter of 1.5 cm combined with a low intrinsic activity ($C_A < 0.8$) do pore diffusion limitations result in a disadvantage for CO conversion (Fig. 5, bottom). However, this effect arises solely due to the assumed limit of the maximum axial temperature (240 °C), which is imposed to prevent excessively high methane selectivity, as shown in Fig. 6.

If the maximum allowable temperature is not restricted, pore diffusion limitations would never result in a lower CO conversion compared to scenarios without such limitations; see blue dashed lines in Fig. 5. The situation for $C_A = 0.8$ (axial profiles of temperature, η_{pore}, and reaction rate), where the same CO conversion is reached in both cases ($\eta_{pore} = 1$ or < 1), is depicted in Supporting Information Fig. S4.

Fig. 6 (for $d_t = 3$ cm) and 7 ($d_t = 1.5$ cm) illustrate the maximum cooling temperature required to ensure safe reactor operation with respect to thermal runaway ($T_{cool} = T_{ignition} - 5$ K) and the corresponding maximum axial temperature (T_{max}). The analysis is presented for both the realistic scenario of pore diffusion limitations ($\eta_{pore} < 1$, shown in blue lines and data points) and the hypothetical case without pore diffusion limitations ($\eta_{pore} = 1$, shown in red).

For cases where the maximum axial temperature that can be reached without risking thermal runaway exceeds 240 °C—such as for a tube diameter of 1.5 cm at any value of the activity coefficient (C_A) under pore diffusion limitations ($\eta_{pore} < 1$)—cooling temperatures that correspond to reaching the 240 °C limit (to avoid excessive methane formation) are also shown (see Fig. 7, bottom).

For a tube size of 3 cm, which is already relatively small for technical multi-tubular FT reactors (typically up to 5 cm in diameter), the temperature level—and consequently the CO conversion (see Fig. 5, top)—achievable under the hypothetical scenario of $\eta_{pore} = 1$—is significantly lower compared to

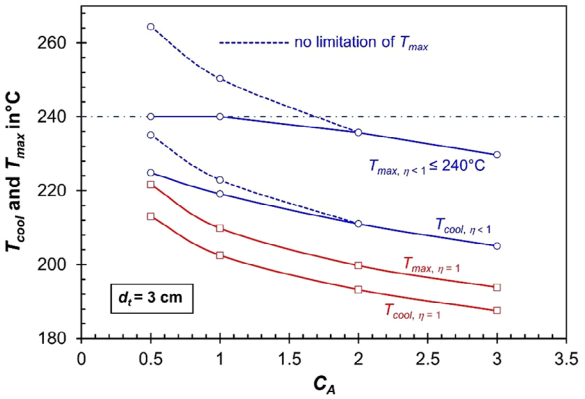

Figure 6. Influence of C_A on the maximum value of the cooling temperature (=$T_{cool,\ ignition}$—5 K) and the corresponding maximum axial temperature (center of tube at $r = 0$) for an (internal) tube diameter of 3 cm. Blue: Realistic consideration of influence of pore diffusion; the dashed blue lines show T_{cool} and $T_{max,\ \eta<1}$, if the maximum allowable temperature would be only limited by thermal runaway (and not by 240 °C with regard to avoid excessive methane formation). Red: hypothetical case without pore diffusion limitations.

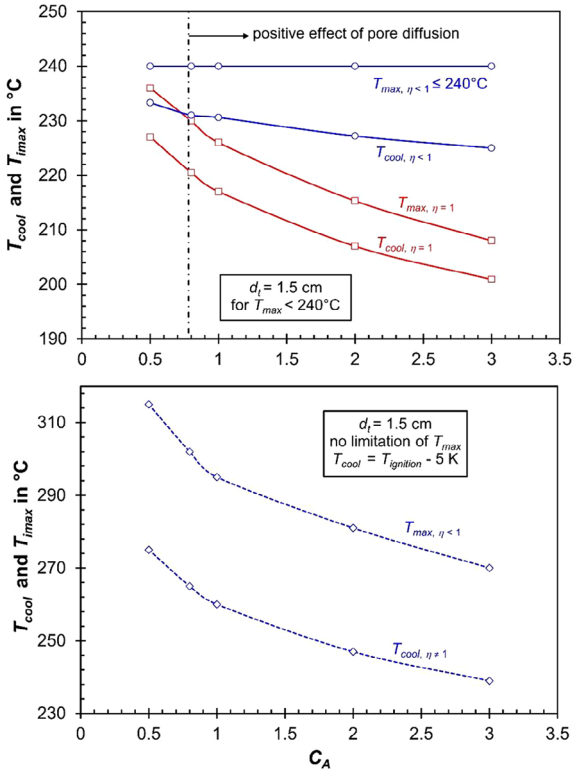

Figure 7. Influence of C_A on the maximum value of the cooling temperature (=$T_{cool,\ ignition}$—5 K) and the corresponding maximum axial temperature (center of tube at $r = 0$) for an (internal) tube diameter of 1.5 cm. Blue: Realistic consideration of influence of pore diffusion; the dashed blue lines in the bottom part show T_{cool} and $T_{max,\ \eta<1}$, if the maximum allowable temperature would be only limited by thermal runaway (and not by 240 °C with regard to avoid excessive methane formation). Red: hypothetical case without pore diffusion limitations. Other reaction/reactor conditions as listed in the Tab. 1 and Supporting Information Tab. S1.

the realistic case of $\eta_{pore} < 1$. This remains true even when the maximum axial temperature is restricted to 240 °C, although higher temperatures would be possible without runaway for $C_A < 2$.

For the very small tube size of 1.5 cm, the temperature level and hence the CO conversion, see Fig. 5, bottom, reached for the hypothetical case of $\eta_{pore} = 1$ gets more and more closer to the "real" case of $\eta_{pore} < 1$, but for realistic values of the activity coefficient C_A of above 0.8, there is still a positive effect of pore diffusion limitations.

Fig. 8 illustrates the impact of temperature on the intrinsic ($r_{CO,\ intr}$) and effective ($r_{CO,\ eff}$) reaction rates under conditions at the reactor entrance ($z = 0$) with fresh syngas for an activity coefficient of $C_A = 3$. The intrinsic reaction rate increases sharply with temperature, corresponding to an apparent activation energy of CO consumption of 148 kJ mol^{-1}. This value results from the parallel formation of methane and C_{2+}-HCs, governed by respective Langmuir–Hinshelwood mechanisms (true activation energies and adsorption enthalpies, see [6]).

For temperatures exceeding 220 °C, the effective activation energy of the effective rate is halved (74 kJ mol^{-1}), as expected, since the pore effectiveness factor (η_{pore}) drops below 0.5 under these conditions (see also Figs. 1 and 9). (For $C_A = 1$, the temperature is about 240 °C to reach this low value of $E_{A,eff}$, see Supporting Information Figs. S6 and S7.)

As highlighted by the arrow in Fig. 8, at a temperature of 240 °C, the effective reaction rate ($r_{CO,eff}$) matches the intrinsic reaction rate ($r_{CO,\ intr}$) for the hypothetical case of no pore diffusion limitations at 219 °C, a temperature 21 K lower. The higher the temperature, the larger this temperature difference becomes where $r_{CO,\ intr}$ equals $r_{CO,eff}$, diminishing the "advantage" of pore diffusion limitations. Conversely, at lower temperatures, this difference decreases, reducing the positive impact of pore diffusion limitations.

It is important to note that the maximum allowable temperature difference (before runaway is likely to occur) is inversely proportional to the activation energy. Consequently, for a given maximum temperature, this difference is approximately at least twice as large in the presence of pore diffusion limitations, making the reactor less sensitive to fluctuations in cooling temperature and other operating conditions. This relationship can be underlined using a simplified, yet valuable formula for the allowable temperature difference between the reaction temperature in the fixed bed and the cooling temperature (here boiling water) required to avoid runaway in a cooled fixed-bed reactor:

$$\Delta T_{max,\ ignition} = T_{max,ax} - T_{max,cool} \approx \frac{R\,T_{max}^2}{E_{A,eff}} \quad (8)$$

where $T_{max,ax}$ and $T_{max,cool}$ represent the maximum reaction temperature and the maximum cooling temperature, respectively, necessary to prevent thermal runaway. This stability criterion, first derived by Barkelew already in 1959 [38], was developed before high-speed computers became available and has since been

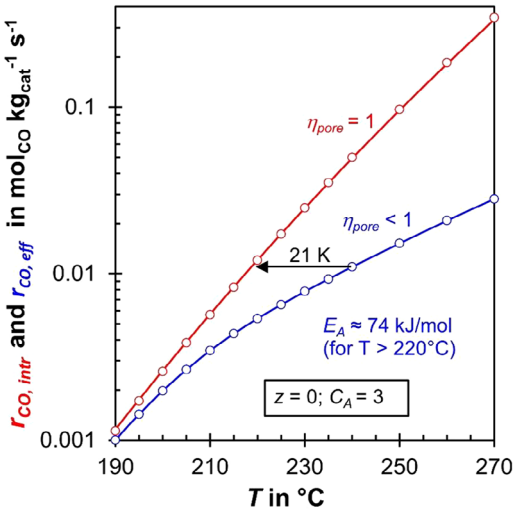

Figure 8. Influence of temperature on intrinsic and effective rate ($r_{CO,\,intr}$ and $r_{CO,\,eff}$). The arrow indicates for the example of $r_{CO,\,eff}$ at 240 °C that this rate is already reached at 219 °C for the hypothetical case without pore diffusion limitations ($r_{CO,\,intr}$) ($C_A = 3$; $z = 0$); conditions as in Tab. 1 and Supporting Information Tab. S1). The respective graph for $C_A = 1$ is shown in Supporting Information Fig. S6.

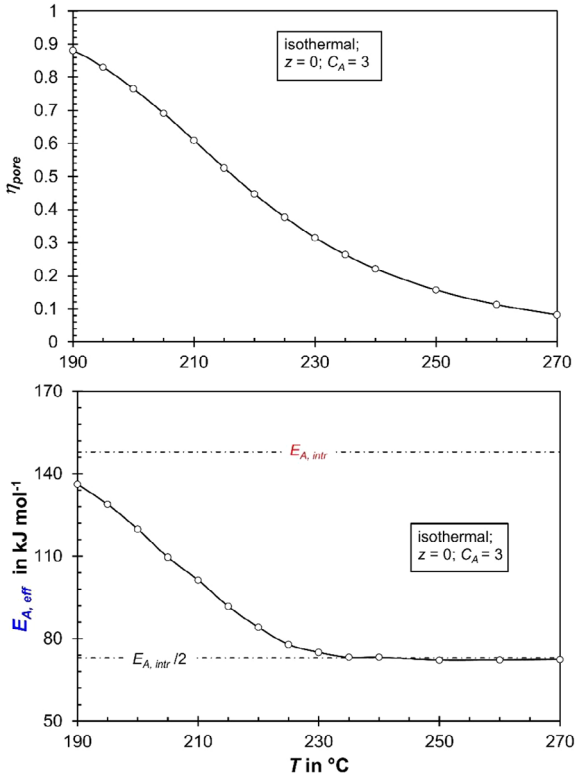

Figure 9. Influence of temperature on pore effectiveness factor and effective activation energy for $C_A = 3$ (reactor entrance ($z = 0$); conditions as listed in Tab. 1 and Supporting Information Tab. S1). The respective figure for $C_A = 1$ is illustrated in Supporting Information Fig. S7.

extensively discussed in the literature, including many textbooks (e.g., [5]).

Although this criterion is a useful guideline, it is slightly conservative, as it is based on the simplifying assumption that the conversion (here of CO) remains negligible at the axial position where the maximum reaction temperature occurs at the center of the fixed bed [5]. In addition, Barkelew only considered in a one-dimensional model approach the temperature difference between the mean reaction temperature and the cooling temperature, i.e., a radial temperature gradient in the bed was neglected. Nevertheless, Eq. (8) shows that the allowable overall radial temperature difference at the position of the axial temperature maximum is inversely proportional to the value of the activation energy (and increases slightly also by a higher temperature level).

Tab. 2 shows the values of $\Delta T_{max,\,ignition}$ ($T_{max,\,r=0} - T_{cool,\,ignition}$) derived from the reactor model for tube diameters of 1.5–3 cm and values of the activity coefficient of 1–3 (entries 1a–8a in Tab. 2). For comparison, the "optimal" temperature differences ($\Delta T_{max,\,opt}$) for cooling temperatures set 5 K below the critical value are also listed (entries 1b–8b). The entries 1–4 represent the hypothetical case of the absence of pore diffusion limitations, whereas the entries 5–8 show the realistic values, including pore diffusion.

The data in Tab. 2 clearly show that $\Delta T_{max,\,ignition}$, and $\Delta T_{max,\,opt}$ are approximately three times higher in the presence of pore diffusion limitations ($\eta_{pore} \neq 1$) compared to cases with negligible influence, i.e., when the intrinsic reaction rate is always reached ($\eta_{pore} = 1$). This trend is consistent when applying the Barkelew approximation (Eq. (8)).

Fig. 10 (dashed lines) illustrates the hypothetical temperature (T_{intr}) that would be required to achieve the same intrinsic reaction rate (hence without pore diffusion limitations) as the effective reaction rate (r_η) observed in the "real" case with pore diffusion limitations. This is shown at the position of the axial temperature maximum ($r = 0$). At this hypothetical temperature T_{intr}, the advantage provided by pore diffusion limitations would disappear, and the "real" CO conversion achieved in the reactor would be nearly identical to the case without limitations.

The "real" modeled values of $T_{intr,max}$, i.e., those reached at the "real" temperature maximum without pore diffusion limitations, are also shown, indicating that these values are in most cases much lower than T_{intr} required to reach r_η. The equality or reversal occurs only for very small tubes (1.5 cm diameter) and at low activity coefficients ($C_A < 1$), see Fig. 10.

It is important to note that the use of FT eggshell catalysts (with the same average cobalt content) is not a recommended option for cooled fixed-bed reactors, as already demonstrated in a previous publication [39]. The reduced influence of pore diffusion in eggshell catalysts significantly increases the reactor's temperature sensitivity, which, in turn, limits the maximum allowable tube diameter and consequently reduces the productivity per tube.

4 Conclusions

This study investigates the impact of pore diffusion limitations on the performance and stability of cooled multi-tubular reactors used in FTS. Although pore diffusion limitations are traditionally

Table 2. Differences (rounded values) between maximum axial temperature T_{max} ($r = 0$) and cooling temperature T_{cool} calculated by reactor model for different tube diameters, values of C_A), and for consideration of pore diffusion limitations ($\eta_{pore} < 1$) or neglection ($\eta_{pore} = 1$).

No.	η_{pore}	C_A	d_t in cm	$T_{cool,\,ignition}$ in °C	T_{max} ($r = 0$) in °C	$\Delta T_{max,\,ignition} = T_{max} - T_{cool,\,ignition}$ in °C
1a	1	3	3	192.5	209.9	17
2a		1		207.5	227.2	20
3a		3	1.5	205.7	225.0	21
4a		1		221.5	241.7	20
5a	<1	3	3	210.0	278.1	68
6a		1		228.0	286.4	58
7a		3	1.5	243.5	304.2	61
8a		1		264.6	331.7	67
No.	η_{pore}	C_A	d_t in cm	$T_{cool,opt}$	T_{max} ($r = 0$) in °C	$\Delta T_{max,\,opt} = T_{max} - T_{cool,opt}$ in °C
1b	1	3	3	187.5	193.8 ($X_{CO} = 13$ %)	6
2b		1		202.5	209.8 ($X_{CO} = 16$ %)	7
3b		3	1.5	200.7	208.0 ($X_{CO} = 37$ %)	7
4b		1		217.0	225.9 ($X_{CO} = 44$ %)	9
5b	<1	3	3	205.0	229.6 ($X_{CO} = 47$ %)	25
6b		1		223.0	250.5 ($X_{CO} = 52$ %[a)])	28
7b		3	1.5	238.5	268.6 ($X_{CO} = 88$ %[a)])	30
8b		1		259.6	293.3 ($X_{CO} = 91$ %[a)])	34

Note: $T_{cool,\,ignition}$ is the cooling temperature, where runaway occurs, see Figs. 2–4. $T_{cool,opt}$ is set to be by 5 K below $T_{cool,\,ignition}$ to keep a safe distance from runaway. For the case of a safe ("optimal") cooling temperature ($T_{cool,\,opt}$), the conversion of CO is also listed. Runaway takes place for $T_{cool} = T_{cool,\,ignition} + 0.1$ K.

a) Note that X_{CO} is unrealistically high, as the maximum axial temperature is higher than the limit of 240 °C with regard to an unwanted high CH_4 selectivity. Values of X_{CO} for $T_{max} = 240$ °C are shown in Fig. 5.

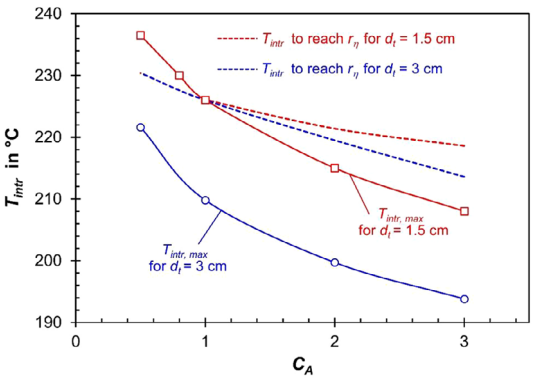

Figure 10. Influence of activity coefficient C_a on the maximum axial temperature $T_{intr,\,max}$ (center of tube at $r = 0$) reached in the front part of the reactor (at $z \approx 3$ m for $d_t = 3$ cm and at $z \approx 1$ m for $d_t = 1.5$ cm; see Figs. 2 and 3) for the hypothetical case without pore diffusion limitations and for (internal) tube diameters of 1.5 and 3 cm. T_{intr} is the temperature, if the intrinsic rate is always reached (i.e., $\eta_{pore} = 1$). The two dashed lines show the values of the maximum axial temperature $T_{intr,\,max}$ that would be needed to reach the same reaction rate as in the realistic case of consideration of the influence of pore diffusion. Note that in case of diffusion limitations, the maximum axial temperature T_{max} is always 240 °C except for $d_t = 3$ cm and $C_a = 2$ (236 °C) and $C_a = 3$ (230 °C) (Fig. 1).

perceived as a drawback, this work demonstrates their significant advantages under typical operational conditions. The reduced temperature sensitivity due to the lower effective activation energy in the presence of pore diffusion limitations enhances reactor stability and allows for higher permissible temperature gradients. This makes the reactor less prone to thermal runaway and more robust against fluctuations in cooling conditions.

Using a 2D numerical model, the analysis reveals that pore diffusion limitations increase the allowable cooling temperature and maximum reaction temperature, improving syngas conversion without compromising safety margins. For realistic cases, the effective reaction rate is reduced to a level where the reactor operates more reliably, achieving higher productivity compared to scenarios without pore diffusion limitations. However, for very small tube diameters and low intrinsic activities, these limitations can occasionally lead to minor reductions in conversion due to constraints imposed by maximum allowable temperatures to limit methane selectivity.

The study also underscores the importance of properly accounting for pore diffusion effects in reactor design and operation. Hypothetical scenarios without pore diffusion limitations show significantly reduced operational stability, requiring stricter control over cooling conditions to avoid runaway.

In conclusion, pore diffusion limitations, often viewed as an unwanted chemical engineering challenge, can act as a stabilizing

factor in cooled fixed-bed reactors for FTS. Only in the up to now rare case of microreactors, discussed for FTS in the last years for small scale and decentralized applications, pore diffusion limitations are a drawback: the channels are very small, only about 1 mm, and thus a very efficient cooling and almost isothermal conditions can be reached [40].

The conclusions derived in this study may also be instructive for other heterogeneously catalyzed exothermic reactions limited by pore diffusion if conducted in cooled fixed-bed reactors. But this should be analyzed by further research also for systems beyond FTS.

Supporting Information

Supporting information for this article can be found under DOI: https://doi.org/10.1002/ceat.70049.

Acknowledgments

Open access funding enabled and organized by Projekt DEAL.

Symbols used

C_A	[–]	Coefficient of catalytic activity (=1 for 10 wt% CO)
c_i	[mol m^{-3}]	Concentration of i (gas phase; i = CO, H_2, H_2O)
C_ϕ	[$kg^{0.5}$ $s^{0.5}$ $m^{-1.5}$]	Constant factor in Eq. (7)
d_t	[m]	(Internal) tube diameter
D	[m^2 s^{-1}]	Diffusion coefficient
$D_{eff,CO,liq}$	[m^2 s^{-1}]	Effective diffusion coefficient of CO in pores filled with liquid HCs
$E_{A,intr}$	[J mol^{-1}]	Intrinsic activation energy ($\eta_{pore} = 1$)
$E_{A,eff}$	[J mol^{-1}]	Effective activation energy < (η_{pore} < 1)
H_{CO}	[Pa m^3 mol^{-1}]	Henry coefficient for CO in liquid HCs
m_{cat}	[kg]	Mass of catalyst
$\dot{n}_{CO}$	[mol s^{-1}]	Molar flux of CO
r	[m]	Radial distance in fixed-bed (r_t = internal radius of tube)
$r_{m,CO}$	[mol_{CO} kg_{cat}^{-1} s^{-1}]	Intrinsic reaction rate of CO
r_{m,CO,H_2O}	[mol_{CO} kg_{cat}^{-1} s^{-1}]	Intrinsic rate of CO, if inhibition by steam is considered
$r_{m,CO,eff}$	[mol_{CO} kg_{cat}^{-1} s^{-1}]	Effective reaction rate of CO to of methane
r_η	[mol_{CO} kg_{cat}^{-1} s^{-1}]	Reaction rate considering pore diffusion limitations
T	[°C, K]	Temperature
X_{CO}	[–]	Conversion of CO
z	[m]	Axial coordinate in fixed-bed

Greek letters

$\Delta_R H_i$	[J mol_{CO}^{-1}]	enthalpy of reaction, I = reaction of CO to methane or to C_{2+}-HCs
ϕ	[–]	Thiele modulus
η_{pore}	[–]	pore effectiveness factor

Abbreviations

C_{2+}	Hydrocarbons with two and more carbon atoms
(—CH_2—)	Methylene group of a normal paraffin
FTS	Fischer–Tropsch synthesis
HC(s)	Hydrocarbon(s)
intr	Related to intrinsic (chemical) reaction rate
SI	Supporting information

References

[1] F. Sauerhöfer-Rodrigo, I. Díaz, M. Rodríguez, P. Pérez, *Rev. Chem. Eng.* **2024**, *40*, 151–192. DOI: https://doi.org/10.1515/revce-2022-0041

[2] J. R. G. Sánchez-López, A. Martínez-Hernández, A. Hernández-Ramírez, *Rev. Chem. Eng.* **2017**, *33* (*2*), 109–142. DOI: https://doi.org/10.1515/revce-2015-0044

[3] C. I. Mendez, J. Ancheyta, F. Trejo, *Energy Fuels* **2017**, *31*, 13011. DOI: https://doi.org/10.1021/acs.energyfuels.7b01431

[4] C. Kern, A. Jess, *Chem. Eng. Technol.* **2009**, *32* (*8*), 1164–1175. DOI: https://doi.org/10.1002/ceat.20090013

[5] A. Jess, P. Wasserscheid, *Chemical Technology: From Principles to Processes*, 2nd ed., Wiley, Weinheim **2020**.

[6] C. Kern, A. Jess, *Catal. Sci. Technol.* **2023**, *13*, 516–527. DOI: https://doi.org/10.1039/D2CY01804G

[7] C. Kern, A. Jess, *Catal. Sci. Technol.* **2023**, *13*, 2212–2222. DOI: https://doi.org/10.1039/D3CY00093A

[8] J. Kern, D. Marrero, C. Urrea, *Processes* **2023**, *11*, 3267. DOI: https://doi.org/10.3390/pr11123281

[9] C. Kern, A. Jess, *Energy Technol.* **2024**, *12*, 2301534. DOI: https://doi.org/10.1002/ente.202301534

[10] C. Kern, A. Jess, *Chem. Eng. Technol.* **2024**, *47*, e202400201. DOI: https://doi.org/10.1002/ceat.202400201

[11] R. Güttel, T. Turek, *Energy Technol.* **2016**, *4*, 44–54. DOI: https://doi.org/10.1002/ente.201500257

[12] F. Pöhlmann, A. Jess, *Energy Technol.* **2016**, *4*, 55–64. DOI: https://doi.org/10.1002/ente.201500216

[13] F. Pöhlmann, A. Jess, *Catal. Today* **2016**, *275*, 172–182. DOI: https://doi.org/10.1016/jcattod.2015.09.032

[14] F. Pöhlmann, S. Rössler, C. Kern, A. Jess, *Catal. Sci. Technol.* **2016**, *6*, 6593–6604. DOI: https://doi.org/10.1039/C6CY00941G

[15] S. Rößler, C. Kern, A. Jess, *Chem. Ing. Tech.* **2018**, *90*, 634–642. DOI: https://doi.org/10.1002/cite.201700142

[16] F. Pöhlmann, *Zusammenspiel von chemischer Reaktion und Porendiffusion bei der kobaltkatalysierten Fischer-Tropsch-Synthese unter Einsatz von CO_2-haltigem Synthesegas*, Ph.D. Thesis, University Bayreuth **2017**.

[17] C. I. Méndez, J. Ancheyta, *Catal. Today* **2023**, *353*, 3–16. DOI: https://doi.org/10.1016/j.cattod.2020.02.012

[18] D. B. Bukur, M. Mandić, B. Todić, N. Nikačević, *Catal. Today* **2020**, *343*, 146–155. DOI: https://doi.org/10.1016/cattod.2018.10.069

[19] E. Iglesia, S. L. Soled, J. E. Baumgartner, S. C. Reyes, *J. Catal.* **1995**, *153*, 108–122. DOI: https://doi.org/10.1006/jcat.1995.1113

[20] J. J. Carberry, D. White, *Ind. Eng. Chem.* **1969**, *61*, 27–35. DOI: https://doi.org/10.1021/ie50715a008

[21] J. G. H. Borkink, K. R. Westerterp, *AIChE J.* **1992**, *38*, 703–715. DOI: https://doi.org/10.1002/aic.690380607

[22] R. W. Fahien, J. M. Smith, *AIChE J.* **1955**, *1*, 28–37. DOI: https://doi.org/10.1002/aic.690010104

[23] M. F. Edwards, J. F. Richardson, *Chem. Eng. Sci.* **1968**, *23*, 109–123. DOI: https://doi.org/10.1016/0009-2509(68)87056-3

[24] W. E. Ranz, *Chem. Eng. Prog.* **1952**, *48*, 247–253.

[25] G. F. Froment, *Ind. Eng. Chem.* **1967**, *59*, 18–27. DOI: https://doi.org/10.1021/ie50686a006

[26] A. G. Dixon, *Chem. Eng. Commun.* **1988**, *71*, 217–237. DOI: https://doi.org/10.1080/00986448808940426

[27] E. Tsotsas, E. U. Schlünder, *Chem. Eng. Sci.* **1988**, *43*, 1200–1203. DOI: https://doi.org/10.1016/0009-2509(88)85081-4

[28] B. D. Kulkarni, L. K. Doraiswamy, *Catal. Rev. Sci. Eng.* **1980**, *22*, 431–483. DOI: https://doi.org/10.1080/03602458008067540

[29] J. J. Carberry, *Chemical and Catalytic Reaction Engineering*, 2nd ed., Dover Publ. Inc, Mineola, New York **2001**.

[30] *VDI-Waermeatlas: Berechnungsblaetter für den Waermeuebergang*, 9th ed. (Ed.: V. D. Ingenieure), Springer-Verlag, Berlin, Heidelberg, Germany **2002**.

[31] E.-U. Schluender, E. Tsotsas, *Waermeuebertragung in Festbetten, durchmischten Schuettguetern und Wirbelschichten*, Georg Thieme Verlag, Stuttgart, Germany **1988**.

[32] M. Nilles, *Waermeübertragung an der Wand durchstroemter Schuettungsrohre*, Ph.D. Thesis, University Karlsruhe, Germany **1991**.

[33] E.-U. Schluender, *Einfuehrung in die Waermeuebertragung*, Vieweg, Braunschweig, Wiesbaden, Germany **1986**.

[34] K. Stephan, *Chem. Ing. Technol.* **1963**, *35*, 775–784.

[35] K. Stephan, *Waermeuebergang beim Kondensieren und beim Sieden*, Springer, Berlin, Heidelberg, New York, London Paris Tokyo **1988**.

[36] W. Fritz, *Chem. Ing. Technol.* **1963**, *35*, 753–764.

[37] S. Ergun, *Chem. Eng. Prog.* **1952**, *48*, 89–94.

[38] C. H. Barkelew, *Chem. Eng. Prog. Symp. Ser.* **1951**, *55*, 37–46.

[39] A. Jess, C. Kern, *Chem. Eng. Technol.* **2012**, *35*, 379–386. DOI: https://10.1002/ceat.201100616

[40] M. Loewert, J. Hoffmann, P. Piermartini, M. Selinsek, R. Dittmeyer, P. Pfeifer, *Chem. Eng. Technol.* **2019**, *42*, 2202–2214. DOI: https://10.1002/ceat.201900136

Research Article: Pore diffusion limitations in Fischer–Tropsch synthesis are typically seen as detrimental due to lower reaction rates. This study shows that they reduce thermal sensitivity and increase reactor stability. A 2D model demonstrates how these limitations enable higher conversions in multi-tubular reactors—turning a drawback into a process advantage.

Pore Diffusion in the Fischer–Tropsch Synthesis: Limitation or Advantage in Multi-Tubular Reactors?

Christoph Kern
Andreas Jess*

Chem. Eng. Technol. **2025**, *48 (7)*, e70049

DOI: 10.1002/ceat.70049

Supporting Information available online

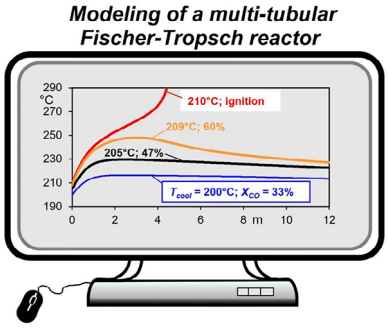

Text for the table of contents
Examples can be found at:
https://onlinelibrary.wiley.com/toc/15214125/0/0